BIOCHEMISTRY
including biophysical chemistry & molecular biology
Article

*Biochemistry* **2010,** *49,* 2585–2592 2585
DOI: 10.1021/bi9019077

# Molecular Level Interactions of S100A13 with Amlexanox: Inhibitor for Formation of the Multiprotein Complex in the Nonclassical Pathway of Acidic Fibroblast Growth Factor†

Sandhya G. Rani, Sepuru K. Mohan, and Chin Yu*

*Department of Chemistry, National Tsing Hua University, Hsinchu, Taiwan*

*Received November 6, 2009; Revised Manuscript Received February 23, 2010*

ABSTRACT: S100A13 and acidic fibroblast growth factor (FGF1) are involved in a wide array of important biological processes, such as angiogenesis, cell differentiation, neurogenesis, and tumor growth. Generally, the biological function of FGF1 is to recognize a specific tyrosine kinase on the cell surface and initiate the cell signal transduction cascade. Amlexanox (2-amino-7-isopropyl-5-oxo-5*H*-[1]benzopyrano[2,3-*b*]pyridine-3-carboxylic acid) is an antiallergic drug that binds S100A13 and FGF1 and inhibits the heat shock induced release of S100A13 and FGF1. In the present study, we investigated the interaction of amlexanox with S100A13 using various biophysical techniques, including isothermal titration calorimetry, fluorescence spectrophotometry, and multidimensional NMR spectroscopy. We report the three-dimensional solution structure of the S100A13−amlexanox complex. These data show that amlexanox binds specifically to the FGF1−S100A13 interface and prevents the formation of the FGF1-releasing complex. In addition, we demonstrate that amlexanox acts as an antagonist of S100A13 by binding to its FGF1 binding site and subsequently inhibiting the nonclassical pathway of these proteins. This inhibition likely results in the ability of amlexanox to antagonize the angiogenic and mitogenic activity of FGF1.

S100A13 is a homodimeric protein that belongs to the S100 subfamily of EF-hand $Ca^{2+}$ binding proteins (*1*−*5*). S100A13 is the only member of the S100 family that has been shown to be involved in the nonclassical export of signal-peptideless proteins, such as fibroblast growth factors, interleukin 1α, and synaptotagmins (*6*−*8*). S100A13 is known to regulate the formation of the acidic fibroblast growth factor and IL-1α multiprotein release complex (*9*). S100A13 is also known to be involved in tumor formation and angiogenesis (*10*−*14*). It is well established that several members of the S100 gene family are associated with the cytoskeleton and that the actin cytoskeleton is essential for transmembrane signaling, endocytosis, and secretion (*15*). FGFs also regulate a wide array of important biological processes, such as cellular differentiation, diabetic retinopathy, rheumatoid arthritis, atherosclerosis, tumor growth, neurogenesis, and embryogenesis (*16*−*19*). FGFs mediate these cellular processes by binding to fibroblast growth factor receptors, which are known as protein tyrosine kinases, on the cell surface (*20*).

S100A13 and FGF1 are exported to the extracellular space through a nonclassical pathway involving the formation of a specific multiprotein complex. The proteins that constitute this complex include S100A13, FGF1, and the p40 form of synaptotagmin1 (syt-1) (*21*−*23*). As S100A13 and FGF1 play important roles in tumor formation, it is clear that preventing the formation of this multiprotein complex is an effective strategy to inhibit a wide range of cancers.

Amlexanox is an antiallergic drug that binds S100A13 and is able to inhibit the heat shock induced release of FGF1 (*6*, *24*, *25*). Amlexanox is mainly an inhibitor of mammalian cell migration and proliferation *in vitro*. The ability of amlexanox to reversibly inhibit human endothelial cell migration and proliferation suggests that its inflammatory activities *in vivo* may possess an antiangiogenic component. Amlexanox induces Src-dependent phosphorylation of cortactin that may be responsible for the reversible inhibition of cell migration and organization of actin stress fibers and induction of Src-dependent cell proliferation (*24*).

A complete understanding of the structural basis of protein function is important for the improvement of pharmacological agents for the treatment of human diseases. S100A13 and FGFs are potentially involved in a wide variety of human pathologies, and the combination of protein engineering with biophysical studies is a useful approach for elucidating the relevant structure−function relationships. The present study aims to increase the understanding of the interactions between S100A13 and amlexanox at the molecular level. We used a variety of biophysical methods, including isothermal titration calorimetry, fluorescence spectroscopy, and multidimensional NMR, to characterize the interactions between S100A13 and amlexanox. Here we report the solution structure of S100A13 with amlexanox using multidimensional NMR spectroscopy. The predicted initial step in the nonclassical pathway is the binding of S100A13 with FGF1 (*26*, *27*). Amlexanox binds in the interface between FGF1 and S100A13, indicating that amlexanox inhibits the formation of the FGF1-releasing complex.

## MATERIALS AND METHODS

*Reagents*. GST-Sepharose was purchased from Amersham Pharmacia Biotech. $^{15}NH_4Cl$, $^{13}C$-labeled glucose, and $D_2O$ were purchased from Cambridge Isotope Laboratories. The components for the Luria broth media were obtained from AMRESCO. Aprotinin, pepstatin, leupeptin, phenylmethanesulfonyl fluoride,

†This research was supported by an operating grant from the National Science Council, Taiwan (NSC 98−2113-M007−018-MY2)
*Corresponding author: e-mail, cyu.nthu@gmail.com; phone, (886)-3-5721524; fax, 886-3-5711082.


Published on Web 02/23/2010

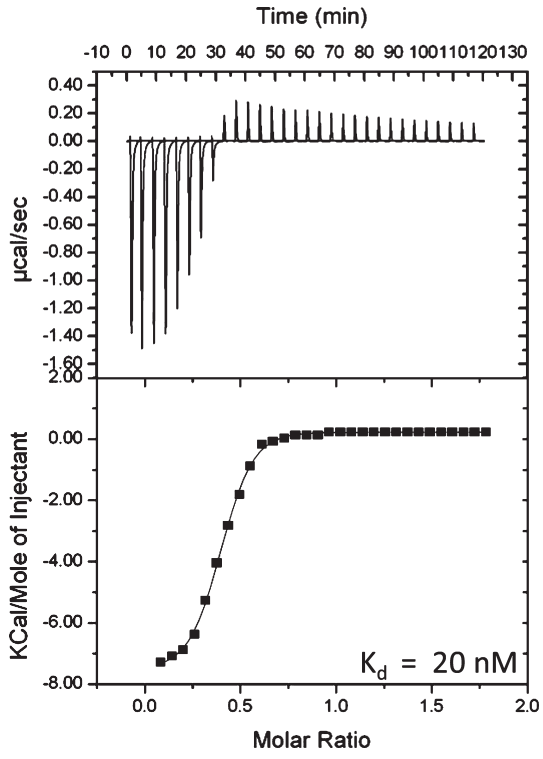


FIGURE 1: Isothermogram representing the binding of S100A13 to amlexanox at 25 °C. The binding constant characterizing the S100A13−amlexanox interaction was 20 nM. The raw data of the titration of S100A13 with amlexanox are shown in the upper panel, while the lower panel shows the integrated data obtained after subtracting the heat of dilution. The titrations were performed in 25 mM PBS (pH 5.6) containing 100 mM NaCl and 2 mM $CaCl_2$. S100A13 concentration was calculated based on monomer S100A13. The concentrations of S100A13 and amlexanox used in ITC experiments are 0.1 and 1.0 mM, respectively.

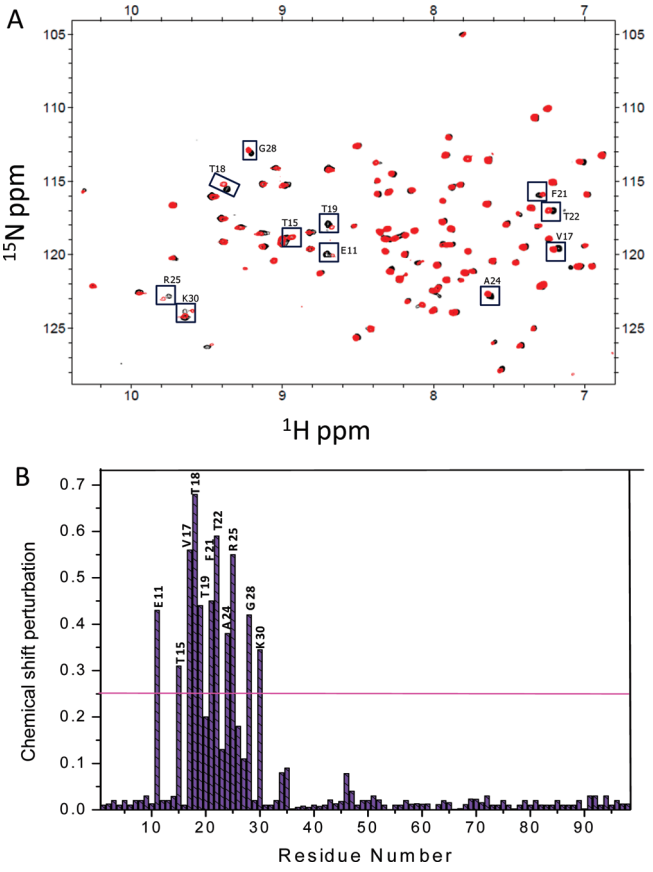


FIGURE 2: Analysis of the free S100A13 and S100A13−amlexanox complex using 2D NMR at a 1:1 binding ratio. (A) The overlaid 2D [$^{1}$H−$^{15}$N]-HSQC spectra highlight the spectral changes of the uniformly $^{15}$N-labeled S100A13 (black) and S100A13 upon binding to amlexanox (red). (B) The weighted average of the chemical shift ($^{1}$H and $^{15}$N) perturbations $\{\Delta\delta = [(\delta^{1}\mathrm{HN})^2 + 0.2(\delta^{15}\mathrm{N})^2]^{1/2}\}$ of the amino acid residues in S100A13 upon complex formation with amlexanox are represented as a bar diagram.

Triton X-100, $\beta$-mercaptoethanol, and amlexanox were all purchased from Water Stone Technology. The Centricon and Amicon membranes were purchased from Millipore. All of the other chemicals used in the study were of high quality analytical grade.

*Protein Expression and Purification*. The cDNA encoding the recombinant protein was subcloned into the pGEX expression vector. Human S100A13 was expressed in *Escherichia coli* [BL21(DE3)]. The unlabeled protein was expressed in Luria broth (LB) medium. The soluble portion of the cell lysate was loaded onto a GST-Sepharose column. Nonspecifically bound proteins were removed by washing the column with PBS buffer. The bound GST-S100A13 protein was eluted with 10 mM glutathione and 50 mM Tris-HCl buffer (pH 8.0). The GST-fused S100A13 protein was exchanged with PBS buffer, and then the solution was treated with 50 $\mu$g of thrombin for 10−12 h to cleave the GST portion of the protein. Then the whole solution was reloaded onto the GST column to obtain pure S100A13. The S100A13 was further purified by gel filtration on a Superdex 75 (Pharmacia) column using an FPLC and 10 mM sodium phosphate (pH 7.0) containing 100 mM NaCl as the eluent. The purity of the protein was checked by SDS−PAGE, and the molecular weight was confirmed by electrospray mass analysis.

*Preparation of $^{15}$N- and $^{13}$C-Labeled S100A13*. The uniform labeling of S100A13 using the isotopes $^{15}$N and $^{13}$C was achieved using M9 minimal medium. This medium contained either $^{15}NH_4Cl$ for single ($^{15}$N) labeling or $^{15}NH_4Cl$ and [$^{13}$C]glucose for double ($^{15}$N and $^{13}$C) labeling of S100A13. The maximum expression yield was achieved using a modified M9 medium that included additional vitamins. The host expression strain, *E. coli* BL21(DE3)pLysS, is a vitamin $B_1$-deficient host, and therefore thiamin (vitamin $B_1$) was added in order to achieve yields up to 10−15 mg/L of the isotope-enriched medium.

*Isothermal Titration Calorimetry* (*ITC*). Protein−ligand binding was characterized by measuring the heat changes during titration of an interacting ligand into a protein solution using a Microcal VP titration calorimeter. Halo S100A13 and amlexanox solutions were centrifuged and degassed under a vacuum before use. Titrations were performed by injecting 8 $\mu$L aliquots of amlexanox (30 times; 1 mM concentration) into 0.1 mM S100A13 solution. The titrations were performed at 25 °C with the protein and ligands dissolved in 25 mM sodium phosphate (pH 5.6) containing 100 mM NaCl and 2 mM $CaCl_2$. Results of the titration curves were corrected using a buffer−protein control and analyzed using the Origin software supplied by Microcal.

*Fluorescence Spectroscopy*. Fluorescence emission spectra were obtained using a Hitachi F-2500 fluorescence spectrophotometer for determination of thermal stability. The protein sample was excited at 280 nm, and the resulting emission spectra were collected at 300 and 350 nm with a slit width of 2.5 nm. The thermal denaturation experiments of the free halo S100A13 and halo S100A13−amlexanox complex were performed at temperatures ranging from 24 to 80 °C at intervals of 4 °C for each data set.

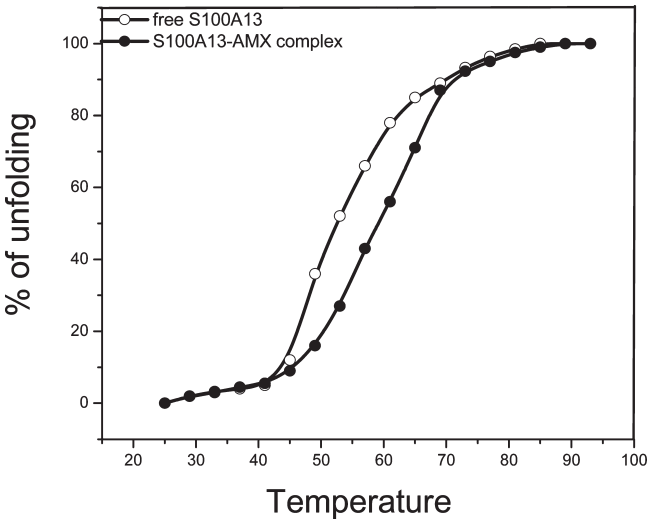


FIGURE 3: Analysis of the thermal stability of S100A13 in the presence and absence of amlexanox. Changes in the fluorescence emission spectra were obtained over a range of wavelengths from 300 to 400 nm. The excitation wavelength was 280 nm, while the emission was monitored at 335 nm with a 2.5 nm slit width.

Table 1: Structural Statistics for the Final 20 Simulated Annealing Structures of S100A13 in the S100A13−Amlexanox Complex

| | |
|---|---|
| **Structural Statistics from ARIA/CNS Restrained Calculations (S100A13 in the S100A13−Amlexanox Complex)** | |
| protein distance restraints | |
| total | 1656 |
| intraresidue | 284 |
| sequential | 391 |
| medium range $1 < \|i-j\| < 5$ | 185 |
| long range $\|i-j\| \geq 5$ | 796 |
| H-bond restraints | 45 |
| dihedral angle restraints | 91 |
| structural statistics for 20 structures | |
| average rmsd | |
| backbone rmsd to mean (Å) | 1.02 ± 0.02 |
| heavy atom rmsd to mean (Å) | 1.23 ± 0.04 |
| average rmsd (structured region) | |
| backbone rmsd to mean (Å) | 0.61 ± 0.02 |
| heavy atom rmsd to mean (Å) | 1.10 ± 0.07 |
| Ramachandran analysis | |
| residues in most favored regions (%) | 77.0 |
| residues in additionally allowed regions (%) | 21.0 |
| residues in generously allowed regions (%) | 1.2 |
| residues in disallowed regions (%) | 0.8 |
| **Structural Statistics from HADDOCK Restrained Calculations (the S100A13−Amlexanox Complex)** | |
| structural statistics for 20 structures | |
| average rmsd at backbone to mean (Å) | |
| average rmsd at S100A13 interface (Å) | 0.58 ± 0.02 |
| average rmsd at amlexanox interface (Å) | 1.29 ± 0.02 |
| Ramachandran analysis | |
| residues in most favored regions (%) | 76.0 |
| residues in additional allowed regions (%) | 21.3 |
| residues in generously allowed regions (%) | 1.6 |
| residues in disallowed regions (%) | 1.1 |

The protein concentration typically was 4 $\mu$M. A Nes Lab circulating water bath was connected to the fluorescence spectrophotometer and used to maintain the desired temperature of the protein sample for the thermal denaturation experiments. In addition, fluorescence analysis of S100A13 showed a typical

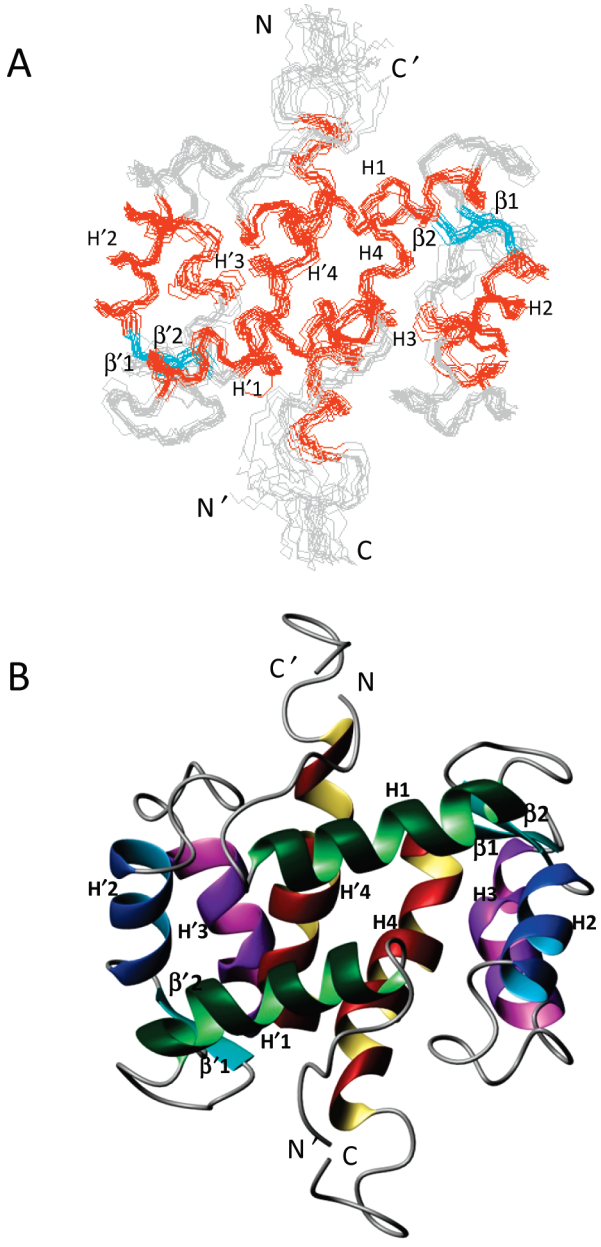


FIGURE 4: (A) Superposition of the backbone (N, $C^{\alpha}$, and C′) atoms of the 20 final solution structures of S100A13 in the S100A13−amlexanox binary complex. The orange, cyan, and gray colors in the figure represent helix, $\beta$-strand, and loop regions, respectively. (B) Ribbon representation of homodimer S100A13 (average structure). Helix 1 is in green, helix 2 is in blue, helix 3 is in violet, helix 4 is in brown, and the two $\beta$-sheets are in cyan in both of the monomers.

spectrum with an emission maximum at 335 nm in its free state and a maximum of 336 nm with significant increase in the intensity in the denatured state based on the environment surrounding the tryptophan residue in S100A13.

*NMR Experiments*. All of the 2D and 3D NMR resonance experiments were performed using a Varian 700 MHz NMR spectrometer equipped with a cold probe at 25 °C. We used halo S100A13 for all of the NMR experiments. The concentration of the protein sample was 1.2 mM in a solution containing 25 mM phosphate (pH 5.6), 2 mM calcium chloride, and 100 mM sodium chloride in the presence of 10% $D_2O$. In the $^{13}$C-filtered NOESY experiment, the spectra of the protein complex were acquired in 100% $D_2O$. The $^{15}$N-labeled protein was titrated with amlexanox at a 1:1 molar ratio in the binary complex. A plot of the weighted

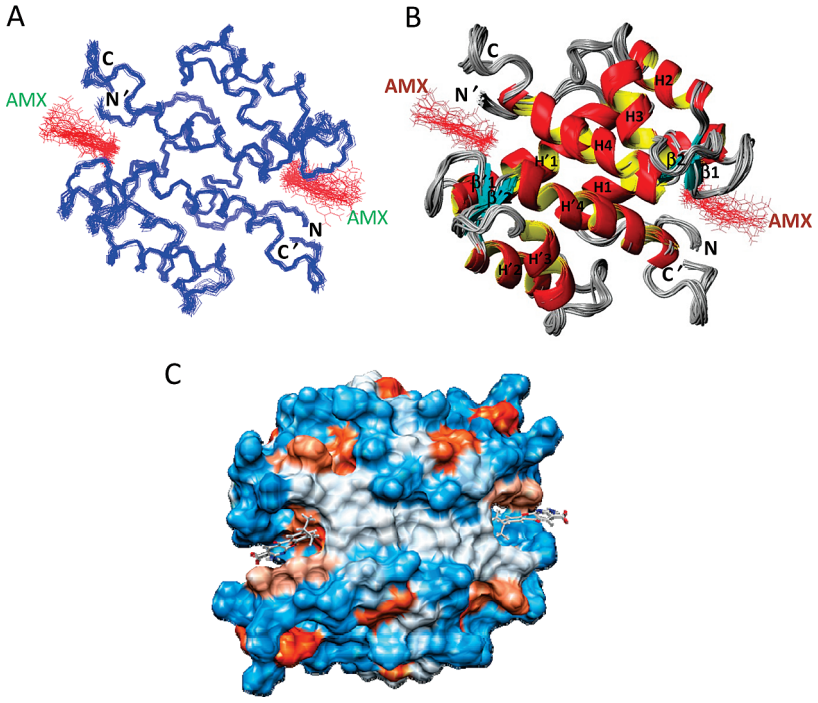


FIGURE 5: HADDOCK structure of the S100A13−amlexanox complex. (A) Overlap of 20 structures showing the backbone representation of the S100A13−amlexanox complex. Amlexanox is colored in red and S100A13 in blue. (B) Ribbon representation of the S100A13−amlexanox complex structure. Amlexanox is shown using the ball and stick representation. (C) Surface representation of the S100A13−amlexanox complex. The orientation of the complex is different from (A) and (B) for better visualization.

average of the $^{15}N$ and $^{1}H$ chemical shift perturbations of the residues of the protein was calculated using the equation $\Delta\delta = [(\delta^{1}H)^2 + 0.2\,(\delta^{15}N)^2]^{1/2}$. All of the spectra were processed using VNMR and analyzed with the Sparky software (*28*).

*3D NMR Experiments*. The S100A13 resonances in the S100A13−amlexanox complex were assigned using various multidimensional NMR experiments. Assignments for the backbone $^{1}H$, $^{13}C$, and $^{15}N$ resonances in the complex were obtained through 3D HNCA and HNCOCA experiments (*29*). The side chain resonances were assigned using 3D $^{15}N$-edited TOCSY-HSQC and HCCH-TOCSY data sets supplemented with other experiments, including CBCACONH (*30*) and HBHACONH (*31*). HNCO spectra were used to assign the carbonyl carbons (*32*). The aromatic resonances of S100A13 were assigned using simultaneous $^{13}C$- and $^{15}N$-edited NOESY-HSQC spectra (*33*). Intermolecular distance restraints were derived from the 3D $^{13}C(\omega_2)$-edited and $^{12}C(\omega_3)$-filtered NOESY-HSQC spectrum (*34*) of 1:1 $^{15}N/^{13}C/^{1}H$ S100A13 and amlexanox (unlabeled).

*Structure Calculation*. The S100A13 complex structure was calculated iteratively using ARIA/CNS (version 2.2) with the PARALLHDG 5.3 force field in the PARALLHDG mode (*35*). We used a variety of triple resonance NMR experiments to solve the solution structure of S100A13 in the S100A13−amlexanox complex. Interproton distance restraints were derived from the NOESY spectrum NOE cross-peak intensities. In addition, information regarding hydrogen bonds was derived from the hydrogen−deuterium exchange experiment, while dihedral angle restraints were generated using TALOS (*36*) with the HN, CA, CB, CO, HA, and HB. A total of 200 structures were calculated and further refined with CNS in an explicit solvent layer of water from which the best 20 structures with the lowest energies were selected. The calculated structures of the protein were analyzed with PROCHECK in order to extract the structural parameters (*37*). MOLMOL and PYMOL were then used for structural representation.

*Molecular Docking*. The S100A13−amlexanox complex was calculated using the docking program HADDOCK (*h*igh *a*mbiguity *d*riven *dock*ing) (*38*−*41*) in combination with CNS (*42*). The amlexanox coordinates were taken from the PDB. The topology and the parameter files were generated using the HIC-UP server (*43*). The docking procedure was driven based on the intermolecular data derived from the $^{13}C(\omega_2)$-edited and $^{12}C(\omega_3)$-filtered NOESY experiment, which was used as restraints in order to dock amlexanox with the ARIA/CNS-derived structure of S100A13. The intermolecular NOE data were used as unambiguous restraints, and the residues that showed chemical shift perturbations were used to define the ambiguous interaction restraints (AIRs) for each residue at the interface region as either an active or a passive residue. We used NACCESS (*44*) in order to determine the solvent-exposed residues in S100A13. Active residues have solvent surface accessible areas that are larger than 50%, while the passive residues have solvent surface accessible areas that are less than 50%.

The docking calculations were performed using HADDOCK 2.0, while the S100A13 (calculated from ARIA/CNS) and the amlexanox parameters were optimized using PARALLELHDG, which included the optimized potentials for liquid simulation (OPLS) parameters for nonbonded interactions (*45*). A total of 5000 structures were calculated, and the 50 structures obtained after water refinement were analyzed. The S100A13−amlexanox binary complex structures were selected based on the structures with the lowest energy conformers.

## RESULTS AND DISCUSSION

Angiogenesis is a cellular process of vital importance during tumor growth or metastasis of cancer. FGF1 is the most crucial angiogenic component in the cell and functions by binding to cell

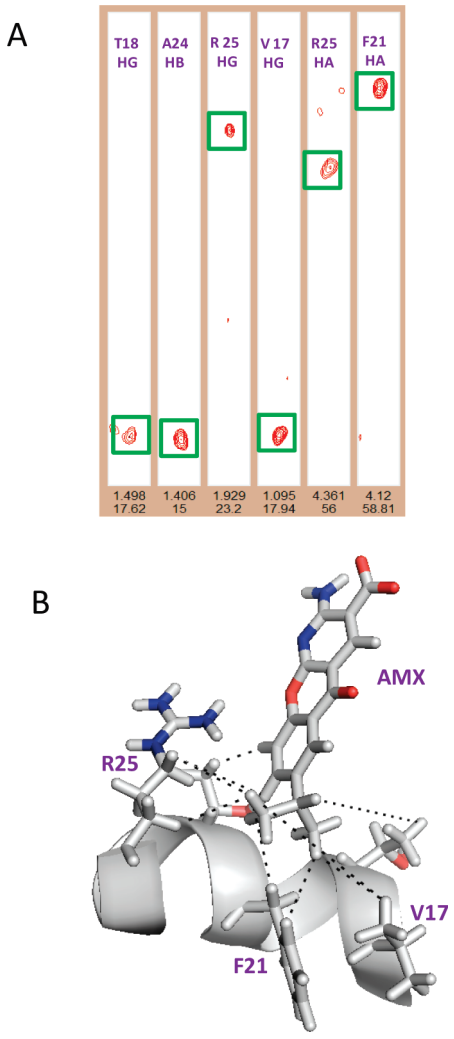


FIGURE 6: Intermolecular NOEs between S100A13 and amlexanox. (A) The intermolecular NOE peaks of the S100A13−amlexanox complex were observed in the $^{13}C(\omega_2)$-edited and $^{12}C(\omega_3)$-filtered NOESY experiment and are represented in strips. The corresponding protons of the S100A13 and amlexanox are labeled in strips. (B) A magnified view of the S100A13−amlexanox complex showing the binding region, and the corresponding residues involved in binding are labeled. The side chains of the residues and the intermolecular interactions between S100A13 and amlexanox are represented using dotted lines.

surface receptors (*46*, *14*). Thus preventing transport of this protein to the extracellular space is an effective strategy to inhibit several types of cancers. Amlexanox is one of the potential antagonists of multiprotein complex formation of FGF1 and S100A13. Thus, elucidation of the interactions between amlexanox and S100A13 at the molecular level would provide information for designing better antagonists of S100A13. In this report, we focused on determining the solution structure of the S100A13−amlexanox complex.

*Isothermal Titration Calorimetry*. ITC is a useful technique to measure the binding constants and energy changes that accompany interactions between proteins and other small ligands (*47*). In this context, we used ITC to analyze S100A13 binding to amlexanox. The equilibrium dissociation constant of the protein−drug interaction was about 20 nM. S100A13−amlexanox binding was defined as a one independent site model, yielding a stoichiometry of binding equal to one amlexanox molecule per monomer of S100A13 (see Figure 1).

*Chemical Shift Perturbation Experiments*. The $^1H-^{15}N$ HSQC spectrum provides a fingerprint of the conformational state of a protein. The ligand binding sites can be easily identified by the chemical shift perturbations of cross-peaks in $^1H-^{15}N$ HSQC spectra. Thus, the comparison of the chemical shift perturbations ($\Delta\delta$) of the free and bound protein is a useful method for identifying the protein−ligand binding interface (*48*). The overlaid $^1H-^{15}N$ HSQC spectra of the free S100A13 and the S100A13−amlexanox complex provide information regarding the amino acid residues of S100A13 that interact with amlexanox. The residues that show the highest chemical shift perturbation hypothetically represent the binding region of amlexanox. Considerable chemical shift perturbations were observed in the overlapped $^1H-^{15}N$ HSQC spectra of the free S100A13 and the S100A13−amlexanox complex at a 1:1 molar ratio (Figure 2A). Residues E11, T15, V17, T18, T19, F21, T22, A24, R25, G28, and K30 showed the maximum chemical shift perturbations (Figure 2B). The cross-peaks in the 2D HSQC spectrum of the S100A13 amino acid residues that shift upon addition of increasing concentrations of amlexanox became saturated at the 1:1 ratio. This indicates a 1:1 binding stoichiometry upon complex formation.

*S100A13 Is Stabilized by the Binding of Amlexanox*. S100A13 contains a single tryptophan residue at position 78 that may be used to monitor conformational changes that occur during protein folding and unfolding. Upon excitation at 280 nm, the emission spectrum of the native protein was dominated by significant fluorescence emission at 334 nm, while the fluorescence emission of the denatured protein decreased significantly at 334 nm. The stability of the protein in the free and binary complex forms can be monitored using this difference in the fluorescence emission. The thermal denaturation of the free S100A13 and the S100A13−amlexanox binary complex was analyzed at temperatures ranging from 24 to 91 °C. This technique is useful for assessing the conformational stability of S100A13 upon binding to amlexanox. The $T_m$ (temperature at which 50% of the protein is in the native form) of the protein increased by 5 °C upon binding of amlexanox, indicating that amlexanox stabilizes S100A13 thermodynamically upon complex formation (Figure 3).

*Solution Structure of the S100A13−Amlexanox Complex*. We have determined the solution structure of the S100A13−amlexanox protein complex using multidimensional NMR techniques. More than 95% of the $^1H$, $^{15}N$, $C^\alpha$, and $C^\beta$ chemical shifts were assigned in this set of analyses. The backbone assignments of the S100A13 amide protons were identified based on the assignments of the S100A13 $^1H-^{15}N$ HSQC resonances. Some of the residues that were difficult to distinguish in the 2D HSQC were identified through the subsequent HNCA experiment. In addition, the $C^\alpha$ and $C^\beta$ resonances were identified by CBCA(CO)NH experiments, while the carbon side chains of the protein binary complex were resolved by the CC(CO)NH experiment. Furthermore, the identities of carbonyl carbons were determined by the HNCO experiment, and the α and $\beta$ proton side chain resonances were resolved by the HBHA(CO)NH experiment. The protons of side chains were assigned from the NMR data obtained from HCCONH and HCCH-TOCSY experiments and from the $^{15}N$-edited NOESY-HSQC spectra. In addition, the $NH_2$ groups of the Gln and Asn amino acid residues were correlated with their $H^\beta$ and $H^\alpha$ protons in the 3D $^{15}N$-edited NOESY spectrum. Chemical shifts of S100A13 and amlexanox are given in the Supporting Information.

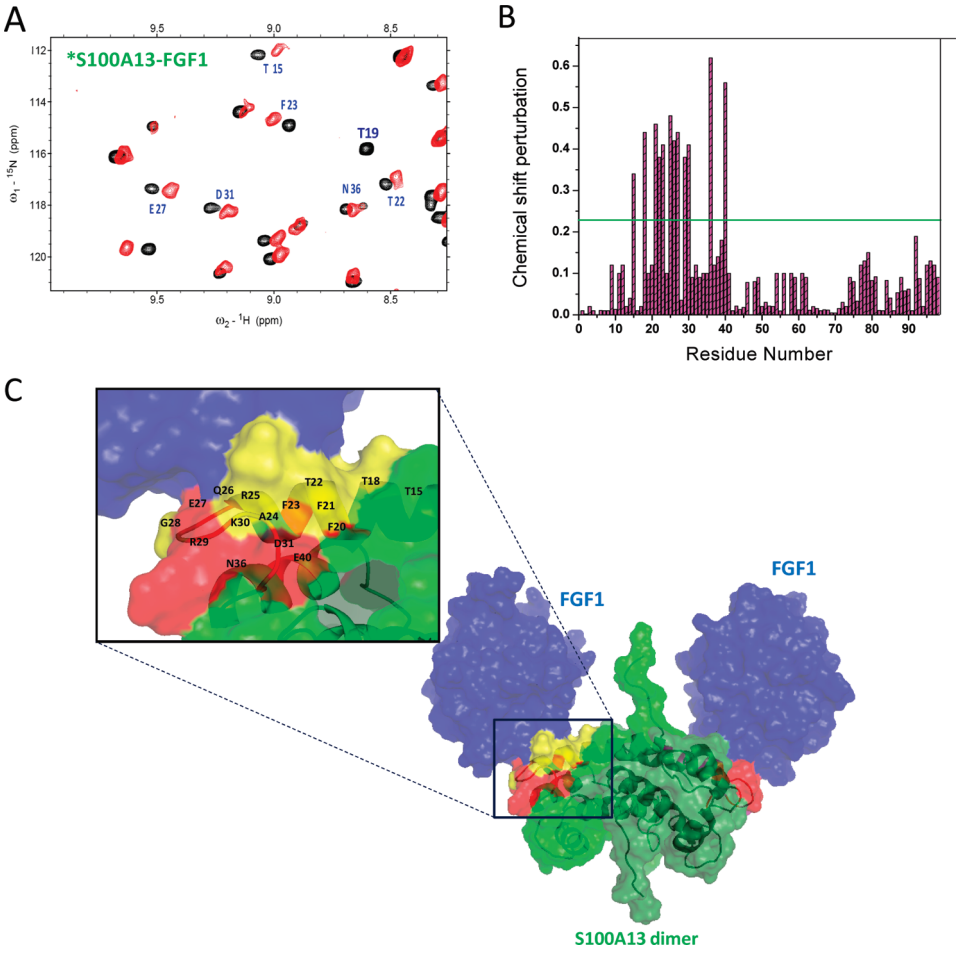


FIGURE 7: (A) Overlapped $^{1}H-^{15}N$ HSQC spectra of S100A13 (uniformly labeled with $^{15}N$) in its free state (black) and in the FGF1-bound state (red). (B) The weighted average of ($^{15}N$ and $^{1}H$) chemical shift perturbation, $\Delta\delta = [(\delta^{1}H)^{2} + 0.2\,(\delta^{15}N)^{2}]^{1/2}$, of residues in S100A13 on complex formation with FGF1. The horizontal line is an arbitrary line drawn to demarcate residues that exhibit significant chemical shift perturbations ( > 0.20 ppm). (C) Surface representation of the FGF1−S100A13 complex. FGF1 is represented in blue, S100A13 is in green, and FGF1 binding sites on S100A13 are in yellow and red. Amlexanox binding sites on S100A13 are represented in yellow. FGF1−S100A13 interface region (red and yellow) was expanded in the magnified view.

Distance restraints were subsequently generated from the $^{15}N$-edited NOESY-HSQC and $^{13}C$-edited NOESY-HSQC data and were used for the structure determination calculations. In addition, hydrogen bond restraints derived by the hydrogen and deuterium exchange experiment were also used for the structure determination. The structural restraints and statistics of the ensemble of the NMR structures calculated by ARIA/CNS are presented in Table 1. Overall, a total of 1656 NOEs were used for the calculation of the S100A13−amlexanox binary complex structure. The calculated structure of the S100A13 protein in the S100A13−amlexanox binary complex agrees well with the NMR structure of the free S100A13 (PDB accession code 1YUU) in the structured region (four α-helices and two $\beta$-sheets) with a backbone rmsd of 1.4 Å. According to a Ramachandran analysis, 76.6% of the residues were in the most favored region and less than 0.9% of the residues were in the disallowed region. The solution structure of the S100A13 in complex was a homodimer, and each monomer contained four α-helices distributed from residues 8−24, 35−45, 56−62, and 73−80 and two $\beta$-sheets located in residues 33−34 and 70−71 (Figure 4).

The S100A13−amlexanox binary complex was calculated using the docking program HADDOCK (Figure 5). In order to determine the complex structure, we used the $^{13}C$-filtered intermolecular NOEs and the chemical shift perturbation data as unambiguous and ambiguous data, respectively. The intermolecular NOEs indicated the presence of five amino acid residues between amlexanox and S100A13 (Figure 6A). The six intermolecular NOEs between amlexanox and S100A13 are illustrated in Figure 6B. The amino acid residues E11, T15, T19, T22, and K30 showed significant chemical shift perturbations; however, no intermolecular NOEs were resolved with these residues in the S100A13−amlexanox binary complex. Residues V17, T18, T22, A24, and R25 had intermolecular NOEs between S100A13 and amlexanox. The ambiguous interaction restraints (AIRs) were subsequently defined for residues that showed a significant chemical shift perturbation in the 2D $^{1}H-^{15}N$ HSQC spectrum. The active and passive residues for the HADDOCK calculations included residues E11, T18, T22, R25, and K30 and residues I13, T19, F20, F21, and G28, respectively, and these residues were in the amlexanox binding region of S100A13. The six intermolecular NOEs that are involved in binding to amlexanox were used for complex structure calculation. The 20 S100A13−amlexanox complex structures with the lowest energies were deposited in the Protein Data Bank (PDB) under the entry code 2kot. The first step in the nonclassical pathway of S100A13 and FGF1 is the formation of the S100A13−FGF1 complex (Yu et al., personal communication, 2009). At a FGF1 (unlabeled):S100A13 ($^{15}N$-labeled) ratio of 1:1, HSQC titration

cross-peaks of S100A13 corresponding to 13 residues, including T15, T18, F21, T22, F23, R25, Q26, E27, R29, K30, D31, N36, and E40, are perturbed upon complexation (Figure 7A,B). These residues constitute the FGF1 binding site(s) in S100A13 as shown in red and yellow color in the inset of Figure 7C. This binding region is distributed in helix 1, loop 1, and helix 2 of S100A13 (Figure 7C). The amlexanox binding residues on S100A13 (T18, T19, F20, F21, T22, A24, R25, G28, K30) are colored in yellow in Figure 7C. This region is part of interface region between S100A13 and FGF1 in the FGF1−S100A13 tetrameric complex (colored in red and yellow). This clearly shows that amlexanox can block the formation of the FGF1-releasing complex.

*Description of the S100A13−Amlexanox Binding Region.* The FGF1 binding site in S100A13 is located in the helix 1 and loop 1 region (Figure 7C). The residues that showed the maximum chemical shift perturbations were observed in this region. In the present study, we identified that amlexanox binds to the side chains of the positive amino acid residues R25 and K30, polar residues T18, T19, and T22, and nonpolar residues I13, V17, F20, and F21 of S100A13. The binding constant of S100A13−amlexanox (20 nM) was stronger than the S100A13−FGF1 binding constant. S100A13 is known to play a key role in FGF1-releasing complex formation and transport of this complex to the extracellular membrane. After binding to amlexanox, S100A13 becomes inactive and cannot participate in FGF1-releasing complex formation; hence, in the presence of amlexanox, FGF1 release is prevented. Recently, our group reported that amlexanox binds to FGF1 and stops formation of the FGF1 dimer in the presence of copper, which is required for the nonclassical pathway of FGF1 (*49*). The amlexanox binding region of FGF1 (residues H117 and Y118) is involved in the S100A13−FGF1 binding interface (*49*). This clearly shows that amlexanox binds both S100A13 and FGF1, which results in inhibition of S100A13−FGF1 complex formation.

The S100 proteins share a high degree of sequence homology (Supporting Information Figure 1) and a common three-dimensional fold. S100 family members display target specificity, suggesting that specific S100 proteins regulate specific cellular processes. S100 functions are associated with a number of human diseases, including cancer, inflammatory disorders, and neurodegeneration. But only some examples of small molecule binding have been reported for S100 family proteins (*50*−*55*). Amlexanox is known to bind with S100A13 and S100A12, but the amlexanox binding region is different in two proteins (*25*). Amlexanox has unique binding site on S100A13.

In this report, we elucidated the structural interactions between S100A13 and amlexanox. These data indicate that amlexanox can prevent the interaction between S100A13 and FGF1, which is crucial for the nonclassical pathway of FGF1. Amlexanox binding to the interface region of S100A13 and its interacting partner is crucial for inhibition of the nonclassical pathway of FGF1. This could be the reason why amlexanox acts as a potential antagonist of the FGF1 nonclassical pathway. These results indicate that amlexanox specifically binds to the FGF1 binding region of S100A13. The interactions between S100A13 and amlexanox are mainly hydrophobic interactions. The elucidation of the solution structure of this binary complex may be useful for improving the current antagonists and possibly designing better antagonists for S100A13 and FGF1.

## ACKNOWLEDGMENT

We thank the 700 MHz Nuclear Magnetic Resonance Facility in the Chemistry Department, National Tsing Hua University.

## SUPPORTING INFORMATION AVAILABLE

Sequence homology of S100 proteins and chemical shifts of S100A13 and amlexanox in the S100A13−amlexanox complex. This material is available free of charge via the Internet at http://pubs.acs.org.

## REFERENCES

1. Kraemer, A. M., Saraiva, L. R., and Korsching, S. I. (2008) Structural and functional diversification in the teleost S100 family of calcium-binding proteins. *BMC Evol. Biol. 8*, 48–48.
2. Chazin, W. J. (2007) The impact of X-ray crystallography and NMR on intracellular calcium signal transduction by EF-hand proteins: Crossing the threshold from structure to biology and medicine. *Science STKE 388*, pe27.
3. Leclerc, E., Fritz, G., Vetter, S. W., and Heizmann, C. W. (2009) Binding of S100 proteins to RAGE: An update. *Biochim. Biophys. Acta 1793* (6), 993–1007.
4. Arnesano, F., Banci, L., Bertini, I., Fantoni, A., Tenori, L., and Vizzoli, M. S. (2005) Structural interplay between calcium(II) and copper(II) binding to S100A13 protein. *Angew. Chem., Int. Ed. 44*, 6341–6344.
5. Ridinger, K., Schafer, B. W., Durussel, I., Cox, J. A., and Heizmann, C. W. (2000) S100A13. Biochemical characterization and subcellular localization in different cell lines. *J. Biol. Chem. 275*, 8686–8694.
6. Carreira, C. M., Lavallee, T. M., Tarantini, F., Jackson, A., Lathrop, J. T., Hampton, B., Burgess, W. H., and Maciag, T. (1998) S100A13 is involved in the regulation of fibroblast growth factor-I and p40 synaptotagmin-1 release in vitro. *J. Biol. Chem. 273*, 22224–22231.
7. Mohan, S. K., Rani, S. G., Kumar, S. M., and Yu, C. (2009) S100A13-C2A binary complex structure—a key component in the acidic fibroblast growth factor for the non-classical pathway. *Biochem. Biophys. Res. Commun. 380*, 514–519.
8. Madinova, A., Soldi, R., Graziani, I., Bagala, C., Bellum, S., Landriscina, M., Tarantini, F., Prudovsky, I., and Maciag, T. (2003) S100A13 mediates the copper-dependent stress-induced release of IL-1a from both human U937 and murine NIH 3t3 cells. *J. Cell Sci. 116*, 2687–2696.
9. Prudovsky, I., Mandinova, A., Soldi, R., Bagala, C., Graziani, I., Landriscina, M., Tarantini, F., Duarte, M., Bellum, S., Doherty, H, and Maciag, T. (2003) The non-classical export routes: FGF1 and IL1a point the way. *J. Cell Sci. 116*, 4871–4881.
10. Landricina, M., Schinzari, G., Lenardo, G. D., Quirino, M., Cassano, A., Argento, E. D., Lauriola, L., Scerrati, M., Prudovsky, I, and Barone, C. (2006) S100A13, a new marker of angiogenesis in human astrocytic gliomas. *J. Neurooncol. 80*, 251–259.
11. Pierce, A., Barron, N., Linehan, R., Ryan, E., Odriscoll, L., Daly, C., and Clynes, M. (2008) Identification of novel, functional role for S100A13 in invasive lung cancer cell lines. *Eur. J. Cancer 44*, 151–159.
12. Hayrabedyan, S., Kyurkchiev, S., and Kehayov, I. (2005) FGF-1 and S100A13 possibly contribute to angiogenesis in endometriosis. *J. Reprod. Immunol. 67*, 87–101.
13. Hsieh, H. L., Schafer, B. W., Weigle, B., and Heizmann, C. W. (2004) S100 protein translocation in response to extracellular S100 is mediated by receptor for advanced glycation endproducts in human endothelial cells. *Biochem. Biophys. Res. Commun. 316*, 949–959.
14. Sparvero, L. J., Asafu-Adjei, D., Kang, R., Tang, D., Amin, N., Im, J., Rutledge, R., Lin, B., Amoscato, A. A., Zeh, H. J., and Lotze, M. T. (2009) RAGE (Receptor for Advanced Glycation Endproducts), RAGE ligands, and their role in cancer and inflammation. *J. Trans. Med. 7*, 17.
15. Schmidt, A., and Hall, M. (1998) Signaling to the actin cytoskeleton. *Annu. Rev. Cell Dev. Biol. 14*, 305–338.
16. Folkman, J. (1995) Angiogenesis in cancer, vascular, rheumatoid and other disease. *Nat. Med. 1*, 27–31.
17. Hayek, A., Culler, F. L., Beattie, G. M., Lopez, A. D., Cuevas, P., and Baird, A. (1987) An in vivo model for study of the angiogenic effects of basic fibroblast growth factor. *Biochem. Biophys. Res. Commun. 147*, 876–880.
18. Nishimura, T., Nakatake, Y, Konishi, M., and Itoh, N. (2000) Identification of a novel FGF, FGF-21, preferentially expressed in the liver. *Biochim. Biophys. Acta 1492*, 203–206.
19. Powers, C. J., Mc Leskey, S. W., and Wellstein, A. (2000) Fibroblast growth factors, their receptors and signalling. *Endocr. Relat. Cancer 7*, 65–97.
20. Jaye, M., Schlessinger, J., and Dionne, C. A. (1992) Fibroblast growth factor receptor tyrosine kinases: Molecular analysis and signal transduction. *Biochim. Biophys. Acta 1135*, 185–199.

21. Landriscina, M., Soldi, R., Bagala, C., Micucci, I., Bellum, S., Tarantini, F., Prudovsky, I., and Maciag, T. (2001) S100A13 participates in the release of fibroblast growth factor 1 in response to heat shock in vitro. *J. Biol. Chem. 276*, 22544–22552.
22. Landriscina, M., Bagala, C., Mandinova, A., Soldi, R., Micucci, I., Bellum, S., Prudovsky, I., and Maciag, T. (2001) Copper induces the assembly of a multiprotein aggregate implicated in the release of fibroblast growth factor 1 in response to stress. *J. Biol . Chem. 276*, 25549–25557.
23. LaValle, T. M., Tarantini, F., Gamble, S., Carreira, C. M., Jackson, A., and Maciag, T. (1998) Synaptotagmin-1 is required for fibroblast growth factor-1 release. *J. Biol. Chem. 273*, 22217–22223.
24. Landriscina, M., Prudovsky, I., Carreira, C. M., Soldi, R., Tarantini, F., and Maciag, T. (2000) Amlexanox reversibly inhibits cell migration and proliferation and induces the src-dependent disassembly of actin stress fibers in vitro. *J. Biol. Chem. 275*, 32753–32762.
25. Shishibori, T., Oyama, Y., Matsushita, O., Yamashita, K., Furuichi, H., Okabe, A., Maeta, H., Hata, Y., and Kobayashi, R. (1999) Three distinct anti-allergic drugs, amlexanox, cromolyn and tranilast, bind to S100A12 and S100A13 of the S100 protein family. *Biochem. J. 338*, 583–589.
26. Graziani, I., Doyle, A., Sterling, S., Kirov, A., Tarantini, F., Landriscina, M., Kumar, T. K., Neivandt, D., and Prudovsky, I. (2009) Protein folding does not prevent the nonclassical export of FGF1 and S100A13. *Biochem. Biophys. Res. Commun. 381*, 350–354.
27. Matsunaga, H., and Ueda, H. (2008) Synergistic $Ca^{2+}$ and $Cu^{2+}$ requirements of the FGF1-S100A13 interaction measured by quartz crystal microbalance: An initial step in amlexanox reversible nonclassical release of FGF1. *Neurochem. Int. 52*, 1076–1085.
28. Goddard, T. D., and Kneller, D. G. SPARKY 3, University of California, San Francisco, CA.
29. Grzesiek, S., and Bax, A. (1992) An efficient experiment for sequential assignment of medium sized backbone isotopically enriched protein. *J. Magn. Reson. B 110*, 201–210.
30. Wittekind, M., and Mueller, L. (1993) HNCACB, a high sensitivity 3D NMR experiment to correlate the amide proton and nitrogen resonances with alpha-carbon and beta-carbon resonances in proteins. *J. Magn. Reson. B 99*, 638–643.
31. Clubb, R. T., Thanabal, V., and Wagner, G. A. (1992) Constant time 3-dimensional triple resonance pulse scheme to intraresidue H-1(N), N-15, C-13(′) chemical shifts in N-15, C-13 enriched proteins. *J. Magn. Reson. 97*, 213–217.
32. Kay, L. E., Xu, G. Y., and Yamazaki, G. (1994) Enhanced-sensitivity triple-resonance spectroscopy with minimal $H_2O$ saturation. *J. Magn. Reson. A 109*, 129–133.
33. Pascal, S. M., Muhandiram, D. R., Yamazaki, T., Forman-Kay, J. D., and Kay, L. E. (1994) Simultaneous acquisition of $^{15}N$- and $^{13}C$-edited NOE spectra of proteins dissolved in $H_2O$. *J. Magn. Reson. B. 103*, 197–201.
34. Breeze, A. L. (2000) Isotope-filtered NMR methods for the study of biomolecular structure and interactions. *Prog. Nucl. Magn. Res. Spectrosc. 36*, 323–372.
35. Rieping, W., Habeck, M., Bardiaux, B., Bernard, A., Malliavin, T. E., and Nilges, M. (2007) ARIA2: Automated NOE assignment and data integration in NMR structure calculation. *Bioinformatics 23*, 381–382.
36. Cornilescu, G., Delaglio, F., and Bax, A. (1999) Protein backbone angle restraints from searching a database for chemical shift and sequence homology. *J. Biomol. NMR 13*, 289–298.
37. Laskowski, R. A., Rullmannn, J. A., MacArthur, M. W., Kaptein, R., and Thornton, J. M. (1996) AQUA and PROCHECK-NMR: Programs for checking the quality of protein structures solved by NMR. *J. Biomol. NMR 8*, 477–486.
38. Dominguez, C., Boelens, R., and Alexandre, M. J. J. B. (2003) HADDOCK: A protein-protein docking approach based on biochemical and/or biophysical information. *J. Am. Chem. Soc. 125*, 1731–1737.
39. De Vries, S. J., van Dijk, A. D. J., Krzeminski, M., van Dijk, M., Thureau, A., Hsu, V., Wassenaar, T., and Bonvin, A. M. J. J. (2007) HADDOCK versus HADDOCK: New features and performance of HADDOCK2.0 on the CAPRI targets. *Proteins: Struct., Funct., Bioinf. 69*, 726–733.
40. Veverka, V., Crabbe, C., Bird, I., Lennie, G., Muskett, F. W., Taylor, R. J., and Carr, M. D. (2008) Structural characterization of the interaction of mTOR with phosphatidic acid and a novel class of inhibitor: Compelling evidence for a central role of the FRB domain in small molecule-mediated regulation of mTOR. *Oncogene 27*, 585–595.
41. Tomaselli, S., Ragona, L., Zetta, L., Assfalg, M., Ferranti, P., Longhi, R., Bonvin, A. M. J. J., and Molinari, H. (2007) NMR-based modeling and binding studies of a ternary complex between chicken liver bile acid binding protein and bile acids. *Proteins: Struct., Funct., Bioinf. 69*, 177–191.
42. Brunger, A. T., Adams, P. D., Clore, G. M., Delano, W. L., Gros, P., Grosse-Kunstleve, R. W., Jiang, J.-S., Kuszewski, J., Nilges, M., Pannu, N. S., Read, R. J., Rice, L. M., Simonson, T., and Warren, G. L. (1998) Crystallography & NMR system: A new software system for macromolecular structure determination. *Acta Crystallogr., Sect. D: Biol. Crystallogr. 54*, 905–921.
43. Kleywegt, G. J. (2007) Crystallographic refinement of ligand complexes. *Acta Crystallogr. 63*, 94–100.
44. Hubbard, S. J., and Thornton, J. M. (1993) NACCESS, Computer Program, Department of Biochemistry and Molecular Biology, University College London.
45. Jorgenson, W. L., and Tirado-Rives, J. (1988) The OPLS (optimized potentials for liquid simulations) potential functions for proteins, energy minimizations for crystals of cyclic peptides and crambin. *J. Am. Chem. Soc. 110*, 1657–1666.
46. Friesel, R., and Maciag, T. (1999) Fibroblast growth factor proto type release and fibroblast growth factor receptor signaling. *Thromb. Haemostasis 82*, 748–754.
47. Pierce, M. M., Raman, C. S., and Nall, B. T. (1999) Isothermal titration calorimetry of protein−protein interactions. *Methods 19*, 213–221.
48. Chang, Y. G., Song, A. X., Gao, Y. G., Shi, Y. H., Lin, X. J., Cao, X. T., Lin, D. H., and Hu, H. Y. (2006) Solution structure of the ubiquitin-associated domain of human BMSC-UbP and its complex with ubiquitin. *Protein Sci. 15*, 1248–1259.
49. Rajalingam, D., Kumar, T. K. S., Soldi, R., Graziani, I., Prudovsky, I., and Yu, C. (2005) Molecular mechanism of inhibition of nonclassical FGF-1 export. *Biochemistry 44*, 15472–15479.
50. Markowitz, J., Chen, I., Gitti, R., Baldisseri, D. M., Pan, Y., Udan, R., Carrier, F., MacKerell, A. D., Jr., and Weber, D. J. (2004) Identification and characterization of small molecule inhibitors of the calcium-dependent S100B-p53 tumor suppressor interaction. *J. Med. Chem. 47*, 5085–5093.
51. Charpentier, T. H., Wilder, P. T., Liriano, M. A., Varney, K. M., Zhong, S., Coop, A., Pozharski, E., Alexander, D., MacKerell, J., Toth, E. A., and Weber, D. J. (2009) Small molecules bound to unique sites in the target protein binding cleft of calcium-bound S100B as characterized by nuclear magnetic resonance and X-ray crystallography. *Biochemistry 48*, 6202–6221.
52. Leon, R., Murray, J. I., Cragg, G., Farnell, B., West, N. R., Pace, T. C. S., Watson, P. H., Bohne, C., Boulanger, M. J., and Hof, F. (2009) Identification and characterization of binding sites on S100A7, a participant in cancer and inflammation pathways. *Biochemistry 48*, 10591–10600.
53. Zhong, S., Macias, A. T., and MacKerell, A. D., Jr. (2007) Computational identification of inhibitors of protein-protein interactions. *Curr. Top. Med. Chem. 7*, 63–82.
54. Garrett, S. C., Hodgson, L., Rybin, A., Toutchkine, A., Hahn, K. M., Lawrence, D. S., and Bresnick, A. R. (2008) A biosensor of S100A4 metastasis factor activation: Inhibitor screening and cellular activation dynamics. *Biochemistry 47*, 986–996.
55. Charpentier, T. H., Wilder, P. T., Liriano, M. A., Varney, K. M., Pozharski, E., MacKerell, A. D., Jr., Coop, A., Toth, E. A., and Weber, D. J. (2008) Divalent metal ion complexes of S100B in the absence and presence of pentamidine. *J. Mol. Biol. 382*, 56–73.